tion mixture was diluted with water (25 times by volume) and filtered through Nucleopore membranes (Whatman, Clifton, NJ) that contained pores 1 μm in diameter. The silver nanocubes could be recovered from ethylene glycol through centrifugation and then redispersed into water.
26. B. D. Cullity, S. R. Stock, *Elements of X–Ray Diffraction* (Prentice-Hall, Upper Saddle River, NJ, ed. 3, 2001), pp. 402–404.
27. Z. L. Wang, *J. Phys. Chem. B* **104**, 1153 (2000).
28. C. Ducamp-Sanguesa, R. Herrera-Urbina, M. Figlarz, *J. Solid State Chem.* **100**, 272 (1992).
29. Z. Zhang, B. Zhao, L. Hu, *J. Solid State Chem.* **121**, 105 (1996).
30. F. Bonet, K. Tekaia-Elhsissen, K. V. Sarathy, *Bull. Mater. Sci.* **23**, 165 (2000).
31. S. J. Oldenburg, R. D. Averitt, S. L. Westcott, N. J. Halas, *Chem. Phys. Lett.* **288**, 243 (1998).
32. W. Lin, T. H. Warren, R. G. Nuzzo, G. S. Girolami, *J. Am. Chem. Soc.* **115**, 11644 (1993).
33. Y. Sun, B. T. Mayers, Y. Xia, *Nano Lett.* **2**, 481 (2002).
34. In a typical procedure for the preparation of gold nanoboxes, a 5-ml aliquot of the aqueous dispersion containing silver nanocubes was refluxed for 10 min. Aliquots of 1 mM $HAuCl_4$ (99.9%, Aldrich) aqueous solution were added dropwise to the refluxing solution. This mixture was continuously refluxed until its color became stable. Vigorous magnetic stirring was maintained throughout the synthesis.
35. Supported in part by the Office of Naval Research (grant N-00014-01-1-0976), a Career Award from NSF (grant DMR-9983893), and a research fellowship from the David and Lucile Packard Foundation. Y.X. is a Camille Dreyfus Teacher Scholar (2002–2007) and an Alfred P. Sloan Research Fellow (2000–2002). We thank D. Qin of the Nanotech User Facility for SEM analysis and X. Jiang, Y. Yin, Y. Lu, B. Mayers, and T. Herricks for their help with electron and x-ray diffraction studies.

12 August 2002; accepted 6 November 2002

Observation of a Strongly Interacting Degenerate Fermi Gas of Atoms

K. M. O'Hara, S. L. Hemmer, M. E. Gehm, S. R. Granade, J. E. Thomas*

We report on the observation of a highly degenerate, strongly interacting Fermi gas of atoms. Fermionic lithium-6 atoms in an optical trap are evaporatively cooled to degeneracy using a magnetic field to induce strong, resonant interactions. Upon abruptly releasing the cloud from the trap, the gas is observed to expand rapidly in the transverse direction while remaining nearly stationary in the axial direction. We interpret the expansion dynamics in terms of collisionless superfluid and collisional hydrodynamics. For the data taken at the longest evaporation times, we find that collisional hydrodynamics does not provide a satisfactory explanation, whereas superfluidity is plausible.

As the fundamental constituents of matter are interacting fermions, the experimental study of strongly interacting, degenerate Fermi gases will have an impact on theories in fields from particle physics to materials science. Although the interactions between fermions are understood when they are weak (e.g., quantum electrodynamics), the treatment of very strong interactions requires the development of new theoretical approaches. Testing these new approaches requires experimental systems with widely tunable interaction strengths, densities, and temperatures. Ultracold atomic Fermi gases have exactly these properties, and thus enable tests of calculational techniques for fundamental systems ranging from quarks in nuclear matter to electrons in high-temperature superconductors (*1–11*). For this reason, a number of groups are developing methods for creating and exploring ultracold atomic Fermi gases (*12–17*). We report on the study of a strongly interacting, degenerate Fermi gas. In contrast to the isotropic expansion previously observed for a noninteracting degenerate Fermi gas (*12*), we observe anisotropic expansion when the gas is released from an optical trap.

An exciting feature of strongly interacting atomic Fermi gases is the possibility of high-temperature superfluids that are analogs of very high temperature superconductors (*8–11*). Our experiments produce the conditions predicted for this type of superfluid transition. Further, the anisotropic expansion we observe has been suggested as a signature of the onset of superfluidity in a Fermi gas (*18*). We interpret the observed anisotropic expansion in terms of both collisionless superfluid hydrodynamics (*18*) and a new form of collisional hydrodynamics.

Strong, magnetically tunable interactions are achieved in our experiments by using a Fermi gas comprising a 50-50 mixture of the two lowest hyperfine states of ^{6}Li, i.e., the $|F = ½, M = ±½\rangle$ states in the low magnetic field basis. This mixture has a predicted broad Feshbach resonance near an applied magnetic field of 860 G (*19, 20*), where the energy of a bound ^{6}Li-^{6}Li molecular state is tuned into coincidence with the total energy of the colliding atoms. This enables the interaction strength to be widely varied (*19–22*). It has also been suggested that interactions between fermions can be modified by immersion in a Bose gas (*23*). Our experiments are performed at 910 G, where the zero-energy scattering length a_S is estimated to be $\sim -10^4\ a_0$ ($a_0 = 0.53 \times 10^{-8}$ cm) and the gas has strongly attractive interactions. Resonance superfluidity has been predicted to occur at this magnetic field for sufficiently low temperatures (*11*).

In our experiments, ^{6}Li atoms are loaded from a magneto-optical trap into an ultrastable CO_2 laser trap (*15*). The trap oscillation frequencies are $\omega_z = 2\pi \times (230 \pm 20$ Hz) for the axial (z) direction and $\omega_\perp = 2\pi \times (6625 \pm 50$ Hz) for the transverse direction. Rate equation pumping is used to produce the 50-50 spin mixture: A broadband radio frequency (rf) field centered at 7.4 MHz is applied at a magnetic field of ~8 G, nulling the population difference according to $\Delta n(t) = \Delta n(0)\ \exp(-2Rt)$, where R is the pumping rate. In our experiments, $2R = 600\ s^{-1}$; applying the rf field for $t = 0.1$ s produces precise population balance.

We achieve very low temperatures via rapid forced evaporation in the CO_2 laser trap. In contrast to experiments that use magnetic traps to achieve degeneracy (*12–14, 16, 17*), this approach has several natural advantages. First, we are able to evaporate both spin states to degeneracy at the desired magnetic field of 910 G. As a result, the sample is never exposed to fields near 650 G where loss and heating are observed (*19, 24*). Second, the evaporation process is identical for both spin states, thereby maintaining the initial spin balance as well as Fermi surface matching. Third, at this field, the collision cross section is extremely large and unitarity-limited, so that runaway evaporation is expected (*25*).

Forced evaporation is achieved by lowering the power of the trapping laser while maintaining the beam profile and angular alignment. The trap depth U is reduced for 3.5 s according to the trajectory $U(t) = U_0(1 + t/\tau)^{-1.45} + U_B$ (*25*), where U_B is a small offset. The value of τ is taken to be 0.1 s, large compared to the time constant estimated for achieving degeneracy at 910 G. With this choice, very high evaporation efficiency is achieved, yielding extremely low temperatures.

After evaporation, the trap is adiabatically recompressed to full depth over 0.5 s and then held for 0.5 s to ensure thermal equilibrium. While maintaining the applied magnetic field of 910 G, the gas is released from the trap and imaged at various times to observe the anisotropy. The CO_2 laser power is extinguished in less than 1 μs with a rejection ratio of 2×10^{-5} (*15*).

Physics Department, Duke University, Durham, NC 27708, USA.

*To whom correspondence should be addressed. E-mail: jet@phy.duke.edu

A charge-coupled device camera images the gas from a direction perpendicular to the axial direction (z) of the trap and parallel to the applied magnetic field direction (y). The small repulsive potential induced by the high-field magnet is along the camera observation axis and does not affect the images. The remaining attractive potential has cylindrical symmetry and corresponds to a harmonic potential with an oscillation frequency for ^{6}Li of 20 Hz at 910 G. Resonant absorption imaging is performed on a cycling transition at a fixed high magnetic field by using a weak ($I/I_{sat} \approx 0.05$), 20-μs probe laser pulse that is σ_- polarized with respect to the y axis. Any residual σ_+ component is rejected by an analyzer. At 910 G, the transitions originating from the two occupied spin states are split by 70 MHz and are well resolved relative to the half-linewidth of 3 MHz, permitting precise determination of the column density and hence the number of atoms per state. The magnification is found to be 4.9 ± 0.15 by moving the axial position of the trap through 0.5 mm with a micrometer. The net systematic error in the number measurement is estimated to be $^{+10\%}_{-6\%}$ (*26*). The spatial resolution is estimated to be ~4 μm by quadratically combining the effective pixel size, 13.0 μm/4.9, with the aperture-limited spatial resolution of ~3 μm.

Figure 1 shows images of the anisotropic expansion of the degenerate gas at various times t after release from full trap depth. The gas rapidly expands in the transverse direction (Fig. 2A) while remaining nearly stationary in the axial direction (Fig. 2B) over a time period of 2.0 ms. In contrast to ballistic expansion, where the column density is $\propto 1/t^2$, the column density decreases only as $1/t$ for anisotropic expansion. Consequently, the signals are quite large even for long expansion times.

One possible explanation of the observed anisotropy is provided by a recent theory of collisionless superfluid hydrodynamics (*18*). After release from the trap, the gas expands hydrodynamically as a result of the force from an effective potential $U_{eff} = \varepsilon_F + U_{MF}$, where $\varepsilon_F(\mathbf{x})$ is the local Fermi energy and $U_{MF}(\mathbf{x})$ is the mean field contribution. In general, $U_{MF} \propto a_{eff}\, n$, where n is the spatial density and a_{eff} is an effective scattering length. However, this theory is not rigorously applicable to our experiment, as it was derived for the dilute limit assuming a momentum-independent scattering length $a_{eff} = a_S$. This assumption is only valid when $k_F|a_S| < 1$, where k_F is the Fermi wave vector. By contrast, our experiments are performed in the intermediate density regime (*7*), where $k_F|a_S| \gg 1$, and the interactions are unitarity-limited. We have therefore attempted to extend the theory in the context of a simple model. We make the assumption that unitarity limits a_{eff} to $\sim 1/k_F$. As $n \propto k_F^3$ and $\varepsilon_F(\mathbf{x}) = \hbar^2 k_F^2/(2M)$, where $\hbar$ is Planck's constant divided by 2π, we obtain $U_{MF} = \beta\varepsilon_F(\mathbf{x})$, where β is a constant. This simple assumption is further justified by more detailed calculations (*7*) showing that β is an important universal many-body parameter. With this assumption, $U_{eff}(\mathbf{x}) = (1 + \beta)\varepsilon_F(\mathbf{x})$. Because $\varepsilon_F \propto n^{2/3}$, it then follows that $U_{eff} \propto n^{2/3}$.

For release from a harmonic trap and $U_{eff} \propto n^\gamma$, the hydrodynamic equations admit an exact solution (*18, 27*),

$$n(\mathbf{x}, t) = [n_0(x/b_x, y/b_y, z/b_z)]/b_x b_y b_z \quad (1)$$

where $n_0(\mathbf{x})$ is the initial spatial distribution in the trap, and $b_i(t)$ are time-dependent scaling parameters that satisfy simple coupled differential equations with the initial conditions $b_i(0) = 1$, $\dot{b}_i(0) = 0$, where $i = x, y, z$. Because the shape of the initial distribution (even with the mean field included) is determined by the trap potential, n_0 is a function only of r' where $\bar{\omega}^2 r'^2 = \omega_\perp^2(x^2 + y^2) + \omega_z^2 z^2$ and $\bar{\omega} = (\omega_\perp^2 \omega_z)^{1/3}$. Hence, the initial radii of the density distribution n_0 are in the proportion $\sigma_x(0)/\sigma_z(0) = \lambda \equiv \omega_z/\omega_\perp$. For our trap, $\lambda = 0.035$. Then, during hydrodynamic expansion, the radii of the density distribution evolve according to

$$\sigma_x(t) = \sigma_x(0) b_x(t)$$
$$\sigma_z(t) = \sigma_z(0) b_z(t) \quad (2)$$

We determine $b_x(t) = b_y(t)$ and $b_z(t)$ from their evolution equations (*18*). For $\gamma = 2/3$, $\ddot{b}_x = \omega_\perp^2 b_x^{-7/3} b_z^{-2/3}$ and $\ddot{b}_z = \omega_z^2 b_x^{-4/3} b_z^{-5/3}$.

From the expansion data, the widths $\sigma_x(t)$ and $\sigma_z(t)$ are determined by fitting one-dimensional distributions (*28*) with normalized, zero-temperature Thomas-Fermi (T-F) distributions, $n(x)/N = [16/(5\pi\sigma_x)](1 - x^2/\sigma_x^2)^{5/2}$. As shown in Fig. 2A, the zero-temperature T-F fits to the transverse spatial profiles are quite good. This shape is not unreasonable despite a potentially large mean field interaction. As noted above, $U_{MF}(\mathbf{x}) \propto \varepsilon_F(\mathbf{x})$. Hence, the mean field simply rescales the Fermi energy in the equation of state (*18*). In this case, it is easy to show that the initial shape of the cloud is expected to be that of a T-F distribution. This shape is then maintained by the hydrodynamic scaling of Eq. 2.

Figure 3A shows the measured values of $\sigma_x(t)$ and $\sigma_z(t)$ as a function of time t after release. To compare these results with the predictions of Eq. 2, we take the initial dimensions of the cloud, $\sigma_x(0)$ and $\sigma_z(0)$, to be the zero-temperature Fermi radii. For our measured number $N = 7.5^{+0.8}_{-0.5} \times 10^4$ atoms per state, and $\bar{\omega} = 2\pi \times (2160 \pm 65$ Hz), the Fermi temperature is $T_F = \hbar\bar{\omega}(6N)^{1/3}/k_B = 7.9^{+0.3}_{-0.2}$ μK at full trap depth. One then obtains $\sigma_x(0) = (2k_B T_F/M\omega_x^2)^{1/2} = 3.6 \pm 0.1$ μm in the transverse direction, and $\sigma_z(0) = 103 \pm 3$ μm in the axial direction. For these initial dimensions, we obtain very good agreement with our measurements using no free parameters, as shown by the solid curves in Fig. 3A.

Figure 3B shows the measured aspect ratios $\sigma_x(t)/\sigma_z(t)$ and the theoretical predictions based on hydrodynamic, ballistic, and attractive ($\beta = -0.4$) or repulsive ($\beta = 0.4$) collisionless mean field scaling (*18*). The observed expansion appears to be nearly hydrodynamic. For comparison, we also show the measured aspect ratios obtained for release at 530 G, where the scattering length has been measured to be nearly zero (*19, 21*). In this case, there is excellent

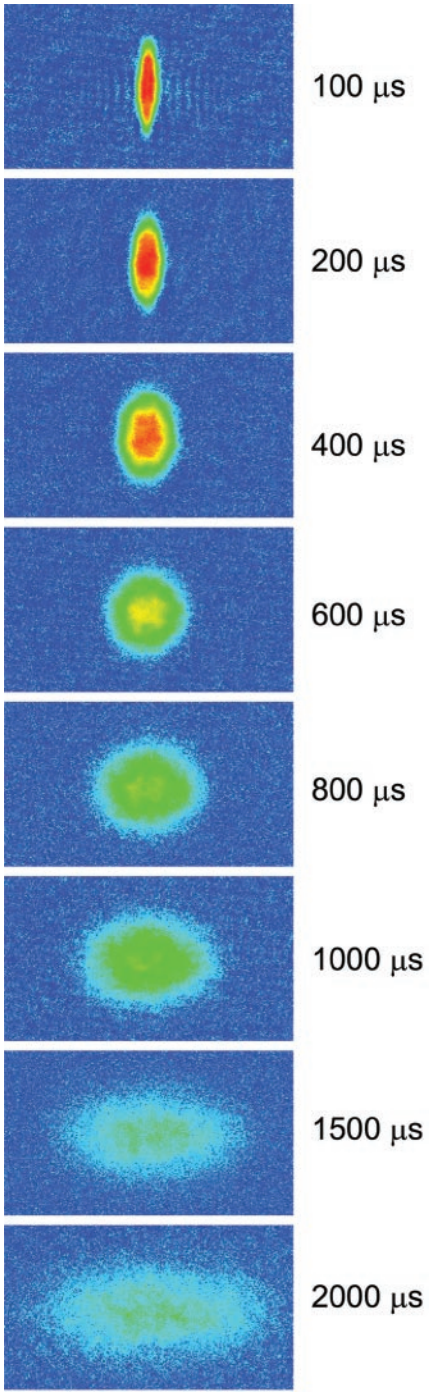

Fig. 1. False-color absorption images of a strongly interacting, degenerate Fermi gas as a function of time t after release from full trap depth for t = 0.1 to 2.0 ms, top to bottom. The axial width of the gas remains nearly stationary as the transverse width expands rapidly.

agreement with the ballistic expansion expected for a noninteracting gas. This directly confirms that the observed anisotropy is a consequence of interactions.

A primary assumption of our simple model is that the system is unitarity limited, i.e., $|k_F a_S| \gg 1$. In this limit the fluid properties are predicted to be independent of $k_F a_S$, both for a collisionless superfluid (*7*) and for collisional hydrodynamics, as shown below (see Eq. 4). To test this assumption, we have released the gas at a trap depth U, which is 1/100 of the full trap depth. Because the trap frequencies, and hence the Fermi energy, scale as $U^{1/2}$, k_F is reduced by $(1/100)^{1/4} \approx 1/3$. The time scale for the expansion is increased by a factor of 10, as expected, and we continue to observe strongly anisotropic expansion. This suggests that the system is unitarity-limited at full trap depth, consistent with the estimated value of $k_F|a_S| = 7.4$ for our experimental conditions. Hence, the gas appears to be strongly interacting.

In the unitarity limit, where $U_{MF} = \beta\varepsilon_F$, we can obtain the first estimate of β from measurements of the transverse release energy. From the zero-temperature T-F fits to the 910 G data, we obtain an average transverse release energy of $\varepsilon_x = \langle Mv^2{}_x/2\rangle = M(\sigma_x/4t)^2 = 1.44 \pm 0.02$ μK per particle. To derive an expression for the release energy as a function of β, we assume that the initial density distribution $n_0(\mathbf{x})$ is determined by the equation of state for a trapped, normal fluid (*18*): $\varepsilon_F(\mathbf{x}) + U_{MF}(\mathbf{x}) + U_{trap}(\mathbf{x}) = \mu$, where μ is the chemical potential. In this case, the release energy per particle is

$$\varepsilon_r = \frac{3}{8} k_B T_F (1 + \beta)^{1/2} \qquad (3)$$

As shown above, $T_F = 7.9^{+0.3}_{-0.2}$ μK at full trap depth. To obtain an estimate of β from the experiments, we assume that $\varepsilon_r/2$ is released in each transverse direction, with negligible energy deposited axially. Calculating β using the appropriate T_F and ε_x for each trial in the range $t = 0.4$ to 0.8 ms, we find $\beta = -0.10 \pm 0.07$. Note that the uncertainty is the quadratic combination of the statistical and systematic uncertainties in the measurements, but does not reflect any systematic effects arising from our model. We find that the sign is in agreement with recent predictions, but the magnitude is smaller than expected by a factor of 10 (*7*). It is remarkable that the release energy and the initial cloud dimensions are well-described assuming a zero-temperature, noninteracting Fermi gas, whereas the highly anisotropic expansion results from strong interactions.

The preceding determination of β assumed a cloud at zero temperature. To investigate the validity of this approximation, we fit normalized, finite-temperature T-F distributions to the transverse data at short times, 0.2 and 0.4 ms, where the signal-to-background ratio in the thermal wings is high. As noted above, it is not unreasonable to expect a T-F distribution. In this case, it is possible to perform a two-parameter fit with σ_x and T/T_F as the free parameters, where T/T_F is the ratio of the temperature to the Fermi temperature. The fits (not shown) to the measured transverse spatial distributions yield $0.08 \leq T/T_F \leq 0.18$, whereas σ_x is essentially unchanged from the zero-temperature results. Hence, it appears that T/T_F is quite small and the zero-temperature approximation is reasonable.

In our experiments, the peak Fermi density is calculated to be $n_F = 4.7 \times 10^{13}/\text{cm}^3$ per state (*29*). At this density, it is possible that the anisotropic expansion arises from collisional hydrodynamics (*27*). In contrast to the case usually considered, for the large scattering lengths in this system, the collision cross section is unitarity-limited to a value $\sigma_F \approx 4\pi/k_F^2$ in the degenerate regime. The gas is collisionally hydrodynamic when the collision parameter $\phi = \gamma/\omega_\perp \gg 1$, where γ is the elastic collision rate and $1/\omega_\perp$ is the relevant time scale for the expansion. Using the s-wave Boltzmann equation (*30*) for a constant cross section σ and including Pauli blocking (*31*), we find that $\gamma = \gamma_0 F_P(T/TF)$, where $\gamma_0 = NM\sigma\bar{\omega}^3/(2\pi^2 k_B T_F)$, N is number of atoms in one spin state, and F_P describes the temperature dependence. Here, $F_P \rightarrow T_F/T$ for $T \gg T_F$, and $F_P \approx 15(T/T_F)^2$ for $T < 0.2T_F$, where Pauli blocking occurs. The maximum value of $F_P = 1.3$ occurs at $T/T_F = 0.5$. In the degenerate regime (i.e., $T < 0.5T_F$), where $\sigma \approx \sigma_F$, we obtain

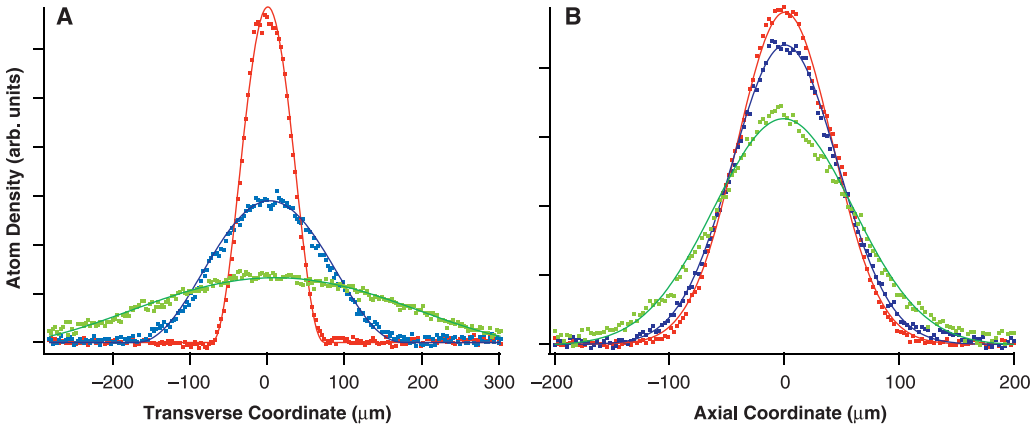

Fig. 2. One-dimensional spatial distributions in the transverse (**A**) and axial (**B**) directions (red, 0.4 ms; blue, 1.0 ms; green, 2.0 ms). The transverse distributions are shown fit with zero-temperature Thomas-Fermi distributions; the axial distributions are shown fit with Gaussian distributions.

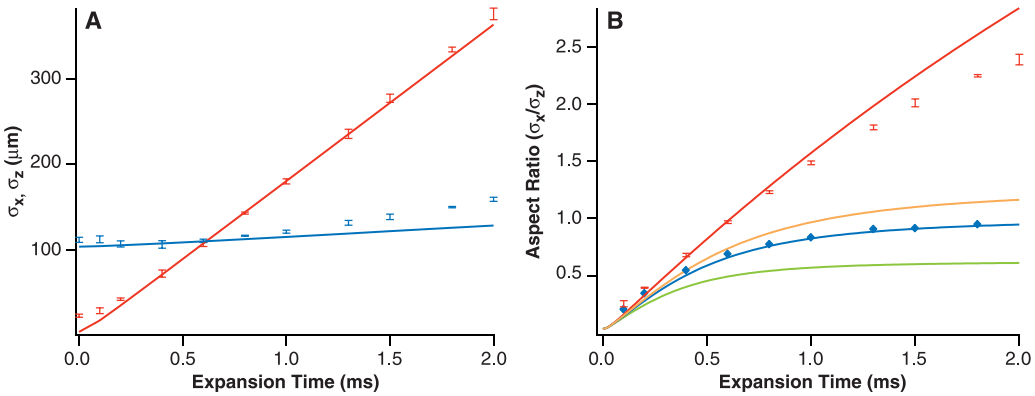

Fig. 3. (**A**) Transverse (red) and axial (blue) widths as functions of time after release. The solid curves are theoretical predictions based on hydrodynamic scaling with no free parameters. (**B**) Aspect ratio of the cloud as a function of time after release. The dots indicate experimental data and the solid curves show theoretical predictions with no adjustable parameters (red, hydrodynamic; blue, ballistic; green, attractive mean field; orange, repulsive mean field).

$$\phi = [(6\lambda N)^{1/3}/6\pi]F_P(T/T_F) \quad (4)$$

For our experimental conditions, $\phi \approx 1.3F_P(T/T_F)$, which is independent of the trap depth as long as $k_F|a_S| \gg 1$. Because F_P is at most of order unity, strongly hydrodynamic behavior arising from collisions seems unlikely. Including the temperature dependence, ϕ ranges from 0.8 down to 0.2 where the system is nearly collisionless. Hence, collisional hydrodynamics does not provide a satisfactory explanation of the observed anisotropic expansion, whereas superfluid hydrodynamics is plausible.

Given this possibility, we have performed an initial investigation of the transition between ballistic and hydrodynamic expansion. We measure the aspect ratio for an expansion time of 0.6 ms as a function of the evaporation time. For short evaporation times < 0.13 s, where $T/T_F > 3.5$, the measured aspect ratio is consistent with that expected for ballistic expansion. For any evaporation time > 1.5 s, the aspect ratio is consistent with hydrodynamic expansion. We observe a very smooth transition between these two extremes. In the intermediate regime, at temperatures below $T/T_F = 3.5$, the expansion lies between hydrodynamic and ballistic. At $T/T_F = 3.5$, where the evaporation time is short and the number is large, an estimate of the classical collision rate with a unitarity-limited cross section shows that the onset of collisional behavior is not surprising. In the intermediate region, there is no theory of expansion to describe the spatial anisotropy of the energy release. Hence, any attempt to determine the temperature is highly model-dependent and cannot be trusted. To further complicate the analysis, varying the evaporation time changes the trap population in addition to the temperature. Finally, if high-temperature resonance superfluidity does exist, the transition temperature is predicted to be in the range 0.25 to 0.5 T_F, where Pauli blocking is not very effective. Hence, one would not expect to observe a collisionless region immediately before the onset of superfluid hydrodynamics, unless the transition occurs at very low temperature, in contrast to predictions.

There are a number of noticeable discrepancies between the hydrodynamic theory and the data. The deviations at 0 and 0.1 ms can be explained by possible index-of-refraction effects as well as spatial resolution limits. These issues are not important for longer expansion times, where the density is reduced and the cloud size is well beyond the resolution limit of our imaging system. However, close examination of the long time deviations reveals that there may be a two-component structure in the gas. In the axial direction, hydrodynamic expansion is very slow, and a second component expanding according to ballistic or collisionless mean field scaling (Fig. 3B) easily overtakes the hydrodynamic component. A two-component structure may also explain why the axial spatial distributions (Fig. 2B) are better fit by Gaussian distributions than by zero-temperature T-F distributions. By contrast, in the transverse direction, the hydrodynamic expansion is the fastest, masking any two-component structure after a short time.

References and Notes

1. P. F. Bedaque, U. van Kolck, available at www.arxiv.org/abs/nucl-th/0203055.
2. W. V. Liu, F. Wilczek, available at www.arxiv.org/abs/cond-mat/0208052.
3. M. Randeria, *Bose-Einstein Condensation*, A. Griffin, D. W. Snoke, S. Stringari, Eds. (Cambridge Univ. Press, Cambridge, 1995), pp. 355–392.
4. H. T. C. Stoof, M. Houbiers, C. A. Sackett, R. G. Hulet, *Phys. Rev. Lett.* **76**, 10 (1996).
5. M. Houbiers *et al.*, *Phys. Rev. A* **56**, 4864 (1997).
6. R. Combescot, *Phys. Rev. Lett.* **83**, 3766 (1999).
7. H. Heiselberg, *Phys. Rev. A* **63**, 043606 (2001).
8. M. Holland, S. J. J. M. F. Kokkelmans, M. L. Chiofalo, R. Walser, *Phys. Rev. Lett.* **87**, 120406 (2001).
9. E. Timmermans, K. Furuya, P. W. Milonni, A. K. Kerman, *Phys. Lett. A* **285**, 228 (2001).
10. Y. Ohashi, A. Griffin, *Phys. Rev. Lett.* **89**, 130402 (2002).
11. S. J. J. M. F. Kokkelmans, J. N. Milstein, M. L. Chiofalo, R. Walser, M. J. Holland, *Phys. Rev. A* **65**, 053617 (2002).
12. B. DeMarco, D. S. Jin, *Science* **285**, 1703 (1999).
13. A. G. Truscott, K. E. Strecker, W. I. McAlexander, G. B. Partridge, R. G. Hulet, *Science* **291**, 2570 (2001).
14. F. Schreck *et al.*, *Phys. Rev. Lett.* **87**, 080403 (2001).
15. S. R. Granade, M. E. Gehm, K. M. O'Hara, J. E. Thomas, *Phys. Rev. Lett.* **88**, 120405 (2002).
16. Z. Hadzibabic *et al.*, *Phys. Rev. Lett.* **89**, 160401 (2002).
17. G. Roati, F. Riboli, G. Modugno, M. Inguscio, *Phys. Rev. Lett.* **89**, 150403 (2002).
18. C. Menotti, P. Pedri, S. Stringari, available at www.arxiv.org/abs/cond-mat/0208150.
19. K. M. O'Hara *et al.*, *Phys. Rev. A* **66**, 041401(R) (2002).
20. M. Houbiers, H. T. C. Stoof, W. McAlexander, R. Hulet, *Phys. Rev. A* **57**, R1497 (1998).
21. S. Jochim *et al.*, *Phys. Rev. Lett.*, in press (available at www.arxiv.org/abs/physics/0207098).
22. T. Loftus, C. A. Regal, C. Ticknor, J. L. Bohn, D. S. Jin, *Phys. Rev. Lett.* **88**, 173201 (2002).
23. G. Modugno *et al.*, *Science* **297**, 2240 (2002).
24. K. Dieckmann *et al.*, *Phys. Rev. Lett.* **89**, 203201 (2002).
25. K. M. O'Hara, M. E. Gehm, S. R. Granade, J. E. Thomas, *Phys. Rev. A* **64**, 051403 (2001).
26. The systematic uncertainty in the number arises from errors in detuning, saturation parameter, and residual optical pumping (which underestimate the true number, as we assume the maximum cross section), as well as errors in the magnification.
27. Y. Kagan, E. L. Surkov, G. V. Shlyapnikov, *Phys. Rev. A* **55**, 18 (1997).
28. Note that the one-dimensional transverse (axial) distributions are obtained by integrating the column density in the axial (transverse) direction.
29. D. A. Butts, D. S. Rokhsar, *Phys. Rev. A* **55**, 4346 (1997).
30. O. J. Luiten, M. W. Reynolds, J. T. M. Walraven, *Phys. Rev. A* **53**, 381 (1996).
31. B. DeMarco, S. B. Papp, D. S. Jin, *Phys. Rev. Lett.* **86**, 5409 (2001).

32. We thank H. Heiselberg and S. Stringari for stimulating correspondence as well as for independently providing us with the release energy formula of Eq. 3. We also thank D. Gauthier for critical reading of the manuscript. Supported by the Chemical Sciences, Geosciences and Biosciences Division of the Office of Basic Energy Sciences, Office of Science, U.S. Department of Energy through a program on the dynamics of ultracold Fermi gases, by NSF through a program on resonance superfluidity, by the Physics Division of the Army Research Office, and by the Fundamental Physics in Microgravity Research program of NASA.

4 October 2002; accepted 31 October 2002
Published online 7 November 2002;
10.1126/science.1079107
Include this information when citing this paper.

Short-Lived Nuclides in Hibonite Grains from Murchison: Evidence for Solar System Evolution

K. K. Marhas,[1] J. N. Goswami,[1]* A. M. Davis[2]

Records of now-extinct short-lived nuclides in meteorites provide information about the formation and evolution of the solar system. We have found excess ^{10}B that we attribute to the decay of short-lived ^{10}Be (half-life 1.5 million years) in hibonite grains from the Murchison meteorite. The grains show no evidence of decay of two other short-lived nuclides—^{26}Al (half-life 700,000 years) and ^{41}Ca (half-life 100,000 years)—that may be present in early solar system solids. One plausible source of the observed ^{10}Be is energetic particle irradiation of material in the solar nebula. An effective irradiation dose of $\sim 2 \times 10^{18}$ protons per square centimeter with a kinetic energy of $\geq$10 megaelectronvolts per atomic mass unit can explain our measurements. The presence of ^{10}Be, coupled with the absence of ^{41}Ca and ^{26}Al, may rule out energetic particle irradiation as the primary source of ^{41}Ca and ^{26}Al present in some early solar system solids and strengthens the case of a stellar source for ^{41}Ca and ^{26}Al.

Pristine early solar system solids recovered from meteorites contain fossil records of several now-extinct short-lived nuclides with half-lives varying from a hundred thousand years to a few tens of millions of years (*1, 2*). Some of these nuclides with short half-lives, such as ^{41}Ca, ^{26}Al, ^{60}Fe [half-life 1.5 million years (My)], and ^{53}Mn (half-life 3.7 My), are considered to be products of stellar nucleosynthesis that were injected into the protosolar cloud